
This is the **accepted version** of the journal article:

Couce-Rios, Almudena; Lledós, Agustí; Fernández, Israel; [et al.]. «Origin of the Anti-Markovnikov Hydroamination of Alkenes Catalyzed by L-Au(I) Complexes : Coordination Mode Determines Regioselectivity». ACS catalysis, Vol. 9, Issue 2 (February 2019), p. 848-858. DOI 10.1021/acscatal.8b03843

This version is available at <https://ddd.uab.cat/record/279251>

under the terms of the  **IN**
COPYRIGHT license

Origin of the anti-Markovnikov hydroamination of alkenes catalyzed by L-Au(I) complexes: coordination mode determines regioselectivity

*Almudena Couce-Rios,^a Agustí Lledós,^{*a} Israel Fernández,^{*b} and Gregori Ujaque^{*a}*

^a Departament de Química and Centro de Innovación en Química Avanzada (ORFEO-CINQA)
Universitat Autònoma de Barcelona, 08193, Cerdanyola del Valles, Catalonia, Spain

^b Departamento de Química Orgánica I and Centro de Innovación en Química Avanzada
(ORFEO-CINQA), Facultad de Ciencias Químicas, Universidad Complutense de Madrid, 28040,
Madrid, Spain

ABSTRACT.

The reaction mechanism and regioselectivity for the gold(I)-catalyzed hydroamination reaction of terminal alkenes are analyzed by means of Density Functional Theory (DFT) calculations. The influence of the nature of the olefin as well as the ligand present in the gold(I) catalyst on the regioselectivity is investigated. The anti-Markovnikov addition is preferred for some alkenes, particularly those having cyclopropyl or good electron-withdrawing groups in their structures. The regioselectivity of the process is quantitatively analyzed with the help of state-of-the-art computational methods, namely the Activation Strain Model (ASM) of reactivity and Natural

Orbitals for Chemical Valence (NOCV) method. It is found that the backbonding interactions in the initially formed π -complex is directly related to the Gibbs energy barrier difference between the Markonikov and anti-Markovnikov additions. It can be concluded that the coordination mode of the initial π -complex ultimately controls the regioselectivity outcome of the transformation.

KEYWORDS

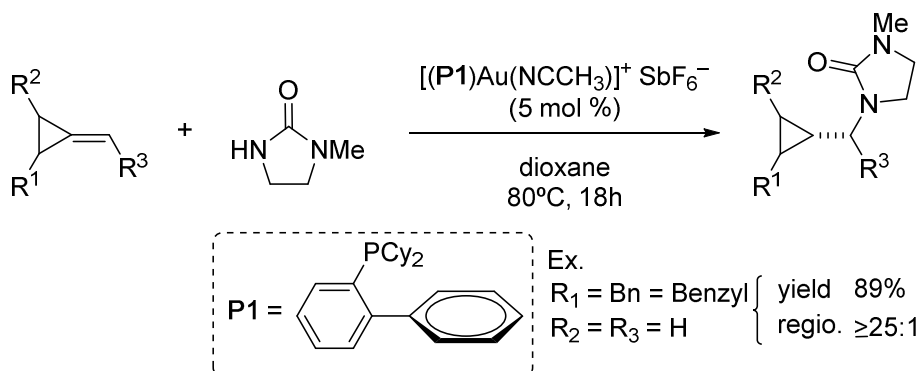
DFT calculations, Gold, Hydroamination, anti-Markovnikov, ASM-EDA(NOCV) analysis

INTRODUCTION

Hydroamination of alkenes is arguably one of the most important and atom-economical methods for the construction of C–N bonds. Several transition metal catalysts have been developed to improve both the efficiency and the selectivity of this transformation,^{1,2,3,4} with gold playing a prominent role, particularly in recent years.⁵ Regarding regioselectivity, the development of a general anti-Markovnikov procedure (listed as one of the ten challenges in catalysis),⁶ is still far from being accomplished, although some examples can be found in the literature.^{7,8} Among them, the recent findings by Widenhoefer's group on the first gold-catalyzed anti-Markovnikov hydroamination reaction of an alkylidenecyclopropane (ACP) substrate should be specially highlighted (Scheme 1).^{9,10}

ACPs are extremely helpful starting building-blocks for the synthesis of functionalized cyclopropanes, since this structural motif is found in a large number of biologically active molecules.¹¹ Remarkably, the hydroamination of the C=C double bond developed by Widenhoefer and co-workers takes place by the nucleophilic addition of the amine at the terminal carbon atom, thus leading to the anti-Markovnikov reaction product. Moreover, whereas most of the methods to

functionalize ACPs involve the simultaneous cyclopropyl C–C bonds cleavage, this procedure overcomes this main synthetic limitation (Scheme 1).

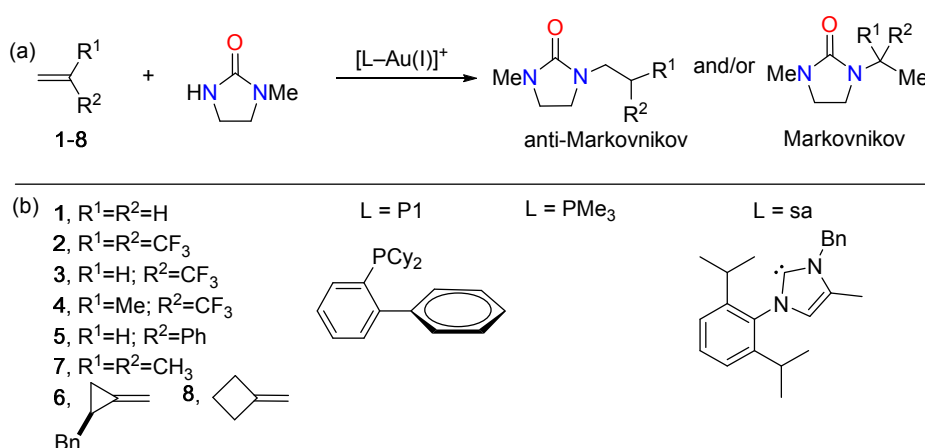


Scheme 1. Gold(I)-catalyzed anti-Markovnikov hydroamination reaction of alkylidenecyclopropanes described by Widenhoefer and co-workers (see ref. ⁹).

In order to understand the regioselectivity of a chemical reaction, the operative reaction mechanism should be first known in detail. Computational investigation is proven to be an extremely useful tool to this end.^{12,13} In this sense, the hydroamination reaction developed by Widenhoefer et al. has been computationally studied by Qi, Xu and coworkers quite recently.¹⁴ The authors analyzed three alternative reaction pathways, namely amine activation, activation of the three-membered ring and the alkene activation. They concluded that the latter pathway is preferred. Therefore, the mechanism involved in this transformation can be generally described as follows: generation of a catalytically active gold(I)– π complex^{15,16} from a gold–chloride precursor, followed by the nucleophilic addition of the N-nucleophile on the activated C=C bond, and final proton migration from nitrogen to carbon atoms. The last step corresponds to the protodeauration reaction of the corresponding alkenyl gold(I) intermediate to generate the observed hydroaminated

product. This proposed pathway is therefore in line with the commonly accepted mechanism for gold-catalyzed nucleophilic additions on unsaturated substrates.¹⁷

Given the importance of developing anti-Markovnikov procedures, and following our interest in rationalizing the transition metal-mediated nucleophilic additions on alkenes,¹⁸ herein we decided to explore in detail the reaction mechanism of this transformation by means of computational methods (Scheme 2a). The influence of both the nature of the substrate and the gold ligand on the reaction outcome was investigated (Scheme 2b). In addition, the origin of the regioselectivity of the process was quantitatively rationalized in terms of the backdonation interactions and geometrical parameters occurring in the initial π -complex.



Scheme 2. (a) Schematic representation of the hydroamination processes studied in this work. (b) substrates and ligands evaluated.

MODELS AND COMPUTATIONAL METHODS

All calculations were carried out using Gaussian 09 program.¹⁹ Calculations were performed at DFT level by means of the M06²⁰ functional with and ultrafine grid option. The basis sets used were the 6-31G(d,p) for all the atoms, except for Au where the SDD (with an additional set of f

polarization functions)²¹ along with the associated pseudopotential was employed. The structures were fully optimized in solution using the SMD²² model with standard parameters and 1,4-dioxane as solvent ($\epsilon=2.2706$). The nature of stationary points (minima and TS) was confirmed by frequency calculations. Connections between the transition states and the minima were checked by following the Intrinsic Reaction Coordinate (IRC)²³ and subsequent geometry optimization till the minima. Energy values given in the text correspond to Gibbs energies at 298K calculated including solvent effects.

EDA-NOCV calculations were carried out using the ADF2017 program²⁴ at the dispersion-corrected BP86²⁵-D3²⁶ level of theory in conjunction with the triple- ζ quality TZ2P basis set²⁷ on the geometries optimized at the M06/6-31G(d,p)&SDD(f) level. Core electrons were described in a frozen-core approximation and the scalar relativistic effects were accounted for using the zeroth-order regular approximation (ZORA).²⁸ This level is therefore denoted ZORA-BP86-D3/TZ2P//M06/6-31G(d,p)&SDD(f).

Calculations have been performed taking the L-gold(I) complex without simplifications in any of the ligands employed: P1= PCy₂(o-biphenyl); Cy=cyclohexyl, PMe₃ and *sa* (see Scheme 2). The structures are named according to the following procedure: ny where n corresponds to the stationary point on the energy profile and y correspond to the Markovnikov (m) or anti-Markovnikov (a) isomer obtained (for example, **2a** corresponds to the second point for the reaction yielding the anti-Markovnikov isomer).

RESULTS AND DISCUSSION

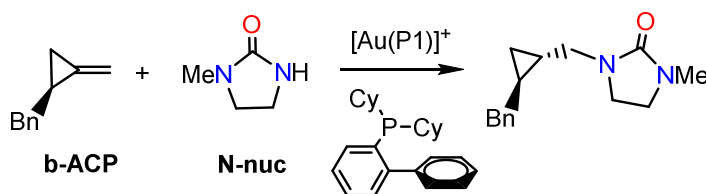
The results are presented in three sections. The first one describes the operative mechanism for the hydroamination reaction of alkylidenecyclopropanes catalyzed by a gold(I) complex with a

phosphine ligand using 1-methyl-imidazolidin-2-one as nucleophile. In the next sections, the influence of both the nature of the substrate and the gold ligand on the process are evaluated by analyzing the hydroamination reactions of eight different alkenes catalyzed by three different gold(I) catalysts having different ligands (P1, PMe₃ and *sa* ligands, Scheme 2).

Analysis of the reaction mechanism

As commented above, the general mechanism for the gold(I) catalyzed hydroamination of alkenes involves the initial generation of a catalytically active gold- π complex from a gold-chloride precursor followed by the nucleophilic addition of the N-nucleophile into the activated carbon-carbon double bond. Then the proton migration from the nitrogen atom to carbon atom takes place followed by the final protodeauration of the alkenyl gold(I) intermediate to generate the reaction product. As commented above, this mechanism was proposed in a previous computational study.¹⁴

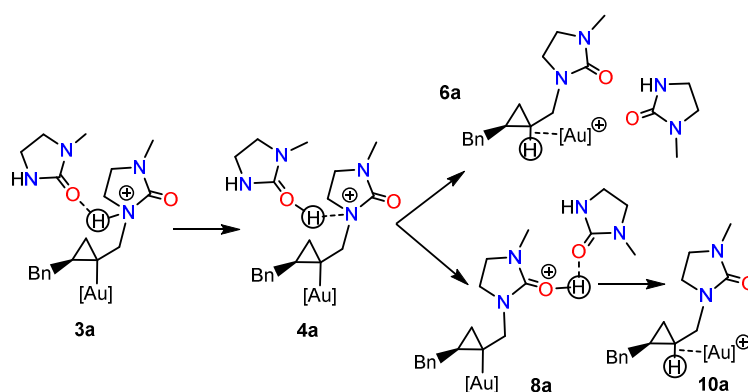
For the sake of completeness, we decided to explore in detail the reaction mechanism for the [Au(P1)]⁺ mediated hydroamination of 1-benzyl-2-methylenecyclopropane, **b-ACP**, with 1-methyl-imidazolidin-2-one, **N-nuc** (Scheme 3).



Scheme 3. Selected Au(I)-catalyzed hydroamination reaction to computationally analyze the mechanism involved in the process.

For analyzing the regioselectivity, the nucleophilic addition over the terminal and internal carbon atoms of the ACP were both explored. The proton migration (protodeauration)²⁹ is known

to be significantly favored by the presence of the counterion or the nucleophile itself.^{18b,30,31} In the previous computational study, it was suggested that for this system the anion assistance can be discarded due to the low basicity of the counteranion, SbF_6^- . An enthalpic barrier of $31.3 \text{ kcal}\cdot\text{mol}^{-1}$ was calculated for the SbF_6^- assisted proton transfer.¹⁴ Herein we explored the nucleophile assistance not considered in the previous work by including a second amine molecule in the model. The intermediate formed upon the initial nucleophilic addition step transfers the proton to the second nucleophile, **4** (Scheme 4). From this intermediate two possibilities can be envisaged, namely the direct proton transfer to the carbon atom generating the product, **6**, or the proton-transfer to the oxygen atom of the bonded urea-based nucleophile, **8**, prior to the protonation of the carbon atom of the alkenyl moiety, **10**. Both possibilities were evaluated for either the Markovnikov or anti-Markovnikov reaction pathways.



Scheme 4. Pathways analyzed for the nucleophile assisted protodeauration process (only the anti-Markovnikov pathway is shown; similar reaction steps were analyzed for the Markovnikov addition).

The Gibbs energy profiles of the four pathways analyzed (i.e. Markovnikov and anti-Markovnikov addition along with the two pathways for the proton transfer described above) are

depicted in Figure 1. The first step of the hydroamination reaction of alkylidenecyclopropane is the N-nucleophilic addition into the gold(I)-coordinated alkene, **1**. The Gibbs energy barriers for the nucleophilic addition step into the terminal and internal carbon atoms of alkene (**TS1_2a** and **TS1_2m**) are 21.0 and 21.7 kcal/mol, with respect to the separated reactants, **1** and **N-nuc**.³² The adducts formed after the Markovnikov and anti-Markovnikov nucleophilic additions (**2m** and **2a**) were located at 13.5 and 20.2 kcal/mol, respectively. The relatively high computed barriers—are then consistent with the temperature used experimentally by Widenhoefer and co-workers (80–100°C).⁹

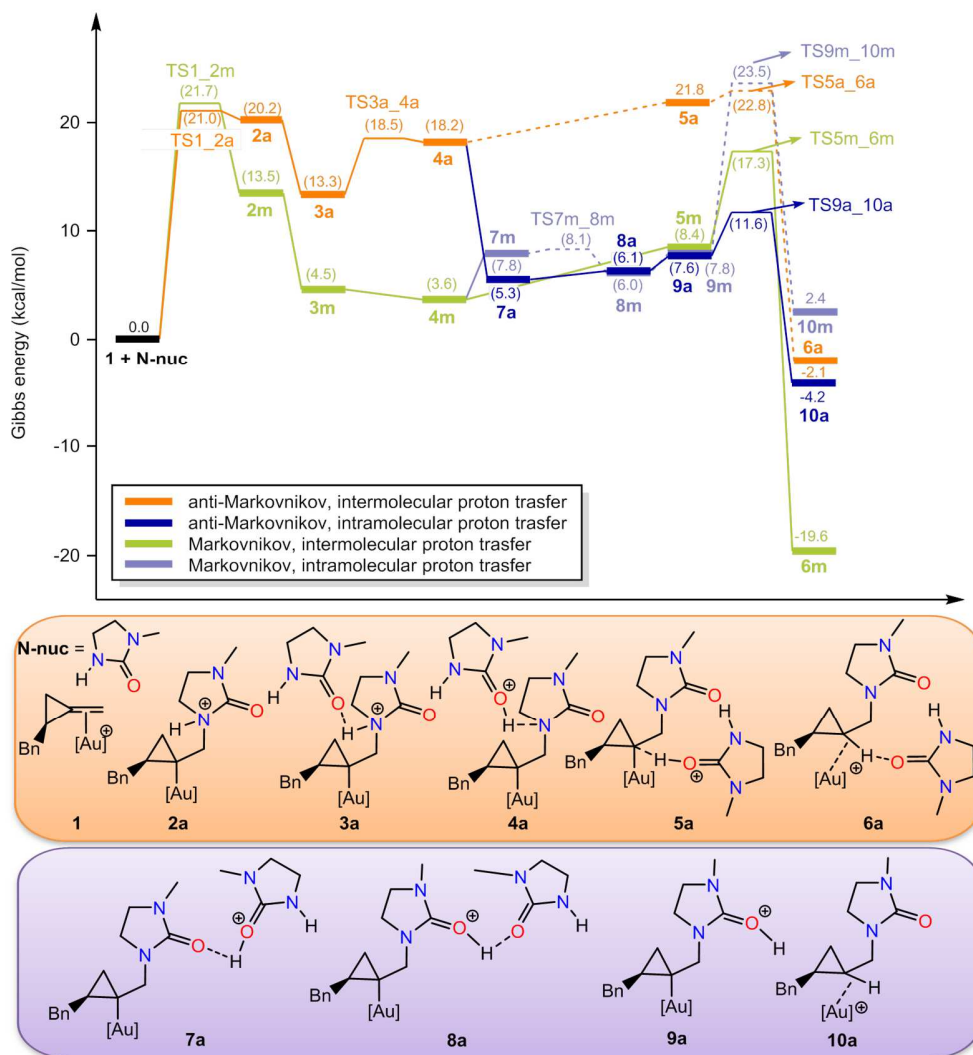


Figure 1. Evaluated reaction profiles for hydroamination of 1-benzyl-2-methylenecyclopropane with 1-methyl-imidazolidin-2-one catalyzed by $[\text{Au}(\text{P1})]^+$ complex. The most plausible mechanism is the so-called “anti-Markovnikov, intramolecular proton transfer”. Relative Gibbs energies (1,4-dioxane solvent, at 298 K, in kcal/mol) were computed at the M06/6-31G(d,p)&SDD(f) level.

For the proton transfer step, we analyzed a pathway including a second amine in the reaction able to act as a proton shuttle. The generated intermediate has a relative Gibbs energy of 13.3 and 4.5 kcal/mol for anti-Markovnikov, **3a**, and Markovnikov, **3m**, additions, respectively. Then a proton transfer from the bonded nucleophile to the oxygen of the second amine molecule takes place to generate intermediates **4** (with relative Gibbs energies of 18.2 and 3.6 kcal/mol for **4a** and **4m**, respectively). At this point the proton can be either transferred to the coordinated carbon atom to generate the product, **6**, or to the oxygen atom of the added nucleophile to generate intermediates **8**, which are then transformed into the final products, **10**. For the anti-Markovnikov addition pathway, the intermediate with the protonated second amine, **4a**, can evolve to intermediate **5a**, located at 21.8 kcal/mol. The transition state associated with the subsequent proton transfer to generate the product, **TS5a_6a**, is located at 22.8 kcal/mol. Alternatively, from **4a** the protonated amine can be reoriented towards the oxygen atom of the bonded amine to form a more stable intermediate, **7a**, and then the proton can be transferred to this oxygen, **8a**; the relative Gibbs energies of these intermediates are 5.3 and 6.1 kcal/mol, respectively. The latter species can evolve to the final coordinated product, **10a**, through transition state **TS9a_10a**; their Gibbs energies are -4.2 and 11.6 kcal/mol, respectively. This pathway is labeled as “anti-Markovnikov intramolecular proton transfer” because the proton migrates from the oxygen atom of the added nucleophile to the carbon atom. The role of the additional nucleophile molecule is therefore to bring the proton

from the N to the O atoms of the bonded nucleophile, Figure 1. The presence of an O center in the nucleophile seems to be crucial in this step. Indeed, a similar hydroamination reactivity to that found for imidazoline-2-ones, has been also reported for 2-pyridones.^{5e,10}

The Gibbs energy profiles clearly show that the proton transfer (protodeauration) is much lower in energy for both, Markovnikov and anti-Markonikov pathways than the initial nucleophilic addition (Figure 1). For the anti-Markovnikov addition, the highest energy transition state for the proton transfer step is located at 11.6 kcal/mol, **TS9a_10a**, with a relative barrier of 6.3 kcal/mol, whereas the nucleophilic addition, **TS1_2a**, is located at 21.0 kcal/mol. According to these results, it can be safely concluded that the nucleophilic addition constitutes the rate determining step (rds) of the entire transformation. In the work of Qi, Yu and co-workers (using a slightly different ACP), they found a direct proton transfer (with an enthalpic energy barrier of ca. 20 kcal/mol).¹⁴ The direct proton transfer in our system gives a Gibbs energy barrier of 28.9 kcal·mol⁻¹. The presence of a second amine molecule, however, significantly reduces the proton transfer barrier for this process (transition state Gibbs energy at 11.6 kcal/mol).

Effect of modifying the alkene's substituents

As the nucleophilic addition constitutes the rate determining step of the process, it can be assumed that the regioselectivity of the transformation is determined by the barrier energy difference ($\Delta\Delta G^\ddagger$) between the anti-Markovnikov and Markovnikov nucleophilic additions. This section is devoted to analyze how the nature of the alkene influences the regioselectivity. To this end, the nucleophilic addition for both Markovnikov and anti-Markovnikov pathways was computed for a set of eight different alkenes (Table 1, see also Scheme 1). Five alkenes, studied experimentally by Widenhoefer, were analyzed: ethylene (entry 1), styrene (entry 5), isobutene

(entry 7), 1-benzyl-2-methylenecyclopropane (**b-ACP**) (entry 6), and methylenecyclobutene (MCB) (entry 8).^{9,5d} For styrene (entry 5), isobutene (entry 7) and methylenecyclobutene (MCB) (entry 8) the formation of the corresponding Markovnikov isomer was favored and only for 1-benzyl-2-methylenecyclopropane (entry 6), the *anti*-Markovnikov reaction product is regioselectively preferred. Unfortunately, the reactions of ethylene (entry 1), styrene (entry 5) and isobutene (entry 7) were carried out experimentally using different ligands, and no experiments with the [Au(P1)]⁺ catalyst are available for a direct comparison.

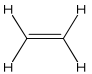
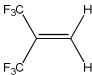
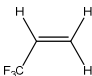
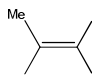
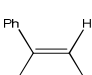
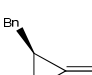

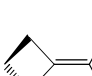
Alkenes including substituents that modify the π -backbonding capacity of the terminal alkene have been also considered: the alkene including the electron withdrawing CF₃ group (entry 3), two CF₃ groups (entry 2) and one CF₃ and one electron donor methyl group (entry 4). The energy barriers for the Markovnikov and anti-Markovnikov additions, as well as the respective energy barrier differences for this series of alkenes are collected in Table 1.

As shown in the previous section, the energy difference between Markovnikov and anti-Markovnikov addition for the process involving **b-ACP** (entry 6) is 0.7 kcal/mol in favor of the anti-Markovnikov adduct.³³ Following the available experimental data, the MCB was also evaluated. For the MCB reactant (entry 8), our calculations give an energy difference of 7.3 kcal/mol in favor of the Markovnikov product, which is fully consistent with the experiments, where no trace of the anti-Markovnikov product was detected.⁹

When isobutene was used as reactant, where both substituents are donating groups (entry 7), the energy difference is 7.0 in favor of the Markovnikov product, once again in agreement with the experimental findings.⁹ At variance, the presence of a CF₃ group (entry 3) clearly favors the anti-Markovnikov addition (energy barrier difference of 8.4 kcal/mol). The strong influence of the

electron withdrawing CF_3 group becomes evident in $(\text{CF}_3)_2\text{C}=\text{CH}_2$ (entry 2), where the regioselectivity was even much more pronounced with an energy barrier difference of 15.1 kcal/mol. Not surprisingly, this effect is somehow attenuated by the presence of a weak donor group (methyl substituent, entry 4), though a clear anti-Markovnikov preference was still found ($\Delta\Delta G^\ddagger = 7.4$ kcal/mol). Finally, our calculations using styrene as substrate predict a 2.0 kcal/mol barrier energy difference favoring the anti-Markovnikov addition.³⁴

Table 1. Gibbs energy barriers (Markovnikov, $\Delta G_{\text{M}}^\ddagger$ and anti-Markovnikov, $\Delta G_{\text{aM}}^\ddagger$, in kcal/mol) for the *anti* nucleophilic attack catalyzed by $[\text{Au}(\text{P1})]^+$ and geometrical parameters (in Å) for their initial intermediates (π -coordinated alkenes).^[a]

Entry	Substrate	$\Delta G_{\text{M}}^\ddagger$	$\Delta G_{\text{aM}}^\ddagger$	$\Delta\Delta G^\ddagger$	$d_1-d_2^{[b]}$
1		15.4	-	-	-0.002
2		23.2	8.1	15.1	0.007
3		19.0	10.6	8.4	-0.002
4		23.5	16.1	7.4	-0.105
5		21.4	19.4	2.0	-0.154
6		21.7	21.0	0.7	-0.119
7		20.4	27.4	-7.0	-0.257
8		20.0	27.3	-7.3	-0.256

^[a] All data have been computed at the M06/6-31G(d,p)&SDD(f) level.

^[b] d_1 =distance Au- $\text{C}_{\text{terminal}}$; d_2 = distance Au- $\text{C}_{\text{internal}}$ from optimized structures.

The activation of an olefin ligand by a metal center toward the nucleophilic addition was qualitatively analyzed by Eisenstein and Hoffmann earlier in the 80s.^{35,36} They realized that the activation of an olefin takes place by a η^2 to η^1 slippage which is also directly related to the shape of the LUMO. Distortion of the ideal position (from symmetric olefins where the distance between the metal and both carbon atoms of the alkene is the same) drives the activation of the olefin. This idea was successfully applied to the nucleophilic addition to Pt(II)-coordinated terminal olefins³⁷ and to the hydroamination of alkenes catalyzed by $[\text{Rh}(\text{DPEphos})]^+$ complex quite recently.³⁸

Figure 2 graphically shows the barrier energy difference between the Markovnikov and anti-Markovnikov addition ($\Delta\Delta G^\ddagger$) versus the difference between the distance for both carbon atoms of the alkene and the metal center (d_1-d_2) in the initial π -coordinate substrate. From the data in Figure 2, it becomes evident that there exists a nice correlation between the $\Delta\Delta G^\ddagger$ and the degree of slippage of the coordinated C=C double bond (correlation coefficient, $R^2 = 0.91$).

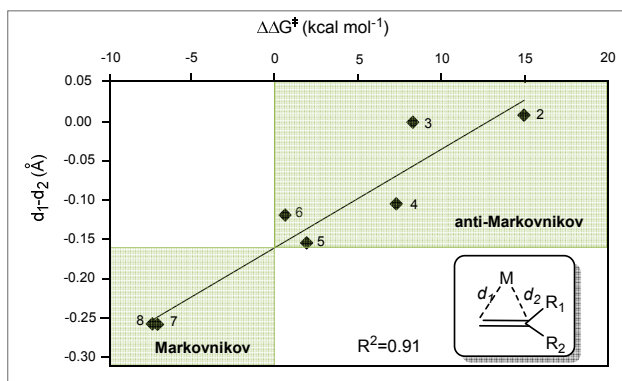


Figure 2. Plot of difference in Gibbs energy between Markovnikov and anti-Markovnikov addition barriers ($\Delta\Delta G^\ddagger$) versus the difference in the distance of both carbon atoms of alkene and the metal center (d_1-d_2 parameter). Values refer to entries in Table 1.

Our calculations therefore suggest that a kinetic parameter ($\Delta\Delta G^\ddagger$) can be correlated to a magnitude that can be directly obtained by knowing the coordination mode of the alkene to the catalyst (an intermediate, that corresponds to a minimum on the potential energy surface). The same conclusion was also obtained for the Rh-catalyzed anti-Markovnikov hydroamination of alkenes.³⁸ This finding may open the door to directly estimate the regioselectivity of the process by simply measuring geometrical parameters of the initial π -coordinate substrate to the catalyst.

The results summarized in Table 1 show that even subtle modifications of the alkene substituents strongly affect the Gibbs energy barriers for the Markovnikov and anti-Markovnikov additions and their energy difference ($\Delta\Delta G^\ddagger$). To gain further quantitative insight into the impact of the substituents in the alkene on the regioselectivity of the process, the Activation Strain Model (ASM)³⁹ of reactivity was applied next. Within this approach, which has enormously contributed to our current understanding of different fundamental transformations,⁴⁰ the potential energy surface $\Delta E(\zeta)$ is partitioned into two contributions along the reaction coordinate ζ , namely the strain $\Delta E_{\text{strain}}(\zeta)$ associated with the deformation (or distortion) experienced by the reactants during the transformation plus the interaction $\Delta E_{\text{int}}(\zeta)$ between these fully deformed reactants (Eq. 1):

$$\Delta E(\zeta) = \Delta E_{\text{strain}}(\zeta) + \Delta E_{\text{int}}(\zeta) \quad (\text{eq. 1})$$

Figure 3 shows the Activation Strain Diagrams (ASDs) for the reaction involving isobutene (which produces the Markovnikov adduct, see Table 1) from the initial π -complexes up to the corresponding transition states, for both the Markovnikov and anti-Markovnikov additions. As readily seen in Figure 3, the ΔE_{strain} term is not at all decisive for the regioselectivity of the process as both nucleophilic approaches requires a nearly identical deformation. Instead, the interaction between the deformed reactants (measured by the ΔE_{int} term) is much stronger for the

Markovnikov pathway along the entire reaction coordinate, which is translated into the lower barrier computed for this approach.

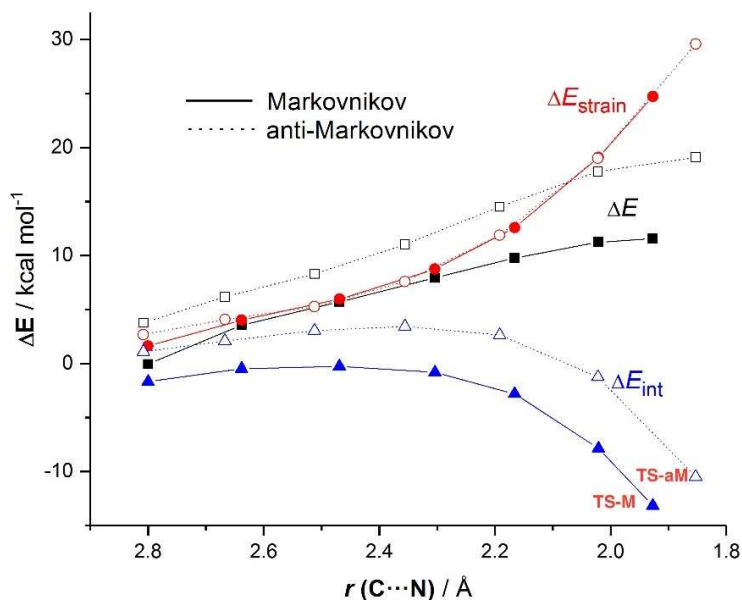


Figure 3. Comparative activation strain diagrams for the gold(I)-catalyzed hydroamination reaction involving isobutene along the reaction coordinate projected onto the forming C...N bond. Markovnikov- and anti-Markovnikov pathways are presented in solid and dotted lines, respectively. All data were computed at the M06/6-31G(d,p)&SDD(f) level.

A markedly different scenario is found for the analogous process involving **b-ACP** (which leads to the formation of the anti-Markovnikov product, see above). As graphically shown in Figure 4, the interaction between the deformed reactants is once again stronger for the Markovnikov pathway along the entire reaction coordinate. However, in this particular case, the π -complex requires a significantly lower deformation energy for the anti-Markovnikov approach as compared to the Markovnikov pathway. This much lower ΔE_{strain} is even able to compensate the stronger interaction energy computed for the Markovnikov pathway, and as a result, the anti-Markovnikov

addition becomes favored. Therefore, it can be concluded that the π -complex formed upon coordination of **b-ACP** to the gold(I)-catalyst already possesses a distorted equilibrium geometry that better fits the transition state structure for the anti-Markovnikov approach. This conclusion is clearly in line with the slippage argument described above.^{35,36}

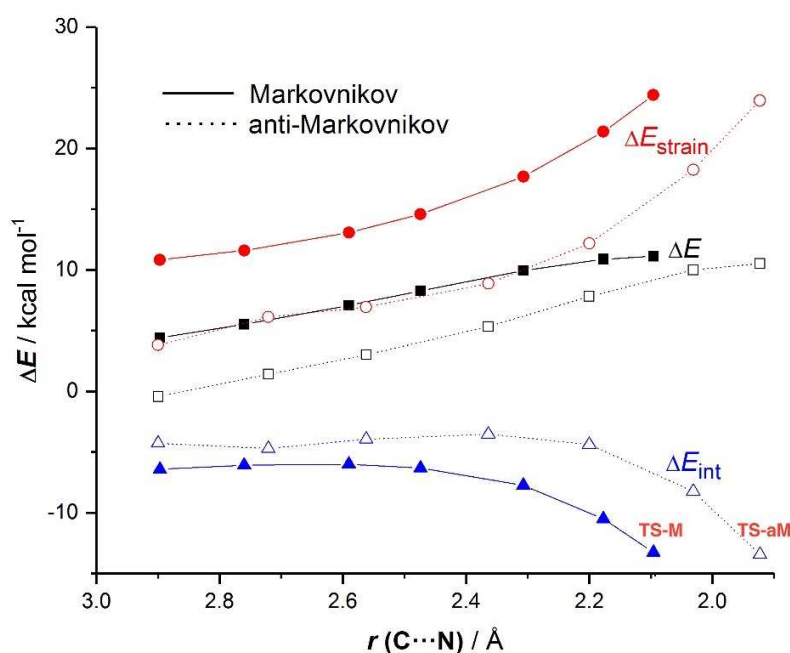


Figure 4. Comparative activation strain diagrams for the gold(I)-catalyzed hydroamination reaction involving **b-ACP** along the reaction coordinate projected onto the forming C \cdots N bond. Markovnikov- and anti-Markovnikov pathways are presented in solid and dotted lines, respectively. All data were computed at the M06/6-31G(d,p)&SDD(f) level.

The distortion induced by the coordination of the alkene to the gold(I)-catalyst should result in significant changes in the electronic structure of the initial cationic alkene- $[\text{Au}(\text{P1})]^+$ π -complexes. To explore this hypothesis, the main orbital contributions present in these species were quantitatively analyzed by means of the NOCV (Natural Orbital for Chemical Valence)⁴¹

extension of the EDA (Energy Decomposition Analysis)⁴² method. The EDA-NOCV approach, which provides pairwise energy contributions for each pair of interacting orbitals to the total bond energy, indicates that two main molecular orbital interactions are present in these π -complexes, namely the donation from the π -molecular orbital of the alkene moiety to the vacant Au–P antibonding orbital of the $[\text{AuP1}]^+$ fragment (denoted as ρ_1) and the backdonation (ρ_2) from a doubly occupied atomic orbital located at the transition metal to the π^* -molecular orbital of the alkene fragment (see Figure 5).⁴³

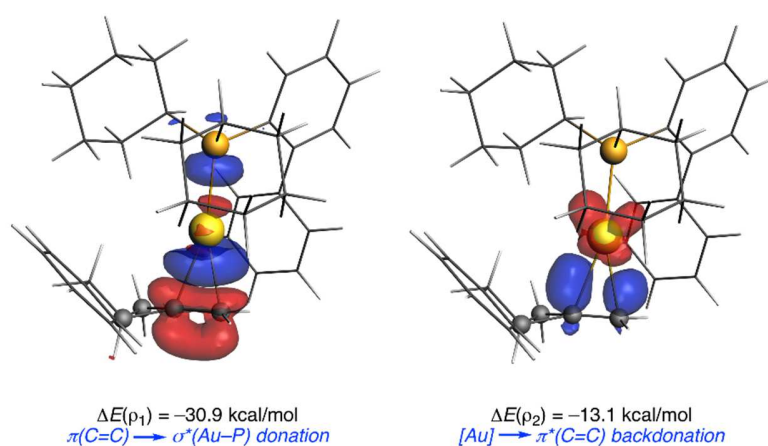


Figure 5. Plot of the deformation densities $\Delta\rho$ of the pairwise orbital interactions present in the $[\text{Au(P1)}]^+ \text{--b-ACP}$ complex and associated stabilization energies $\Delta E(\rho)$. The color code of the charge flow is red \rightarrow blue. Data computed at the ZORA-BP86-D3/TZ2P//M06/6-31G(d,p)&SDD(f) level (isosurface value of 0.002 au).

Not surprisingly, the direct donation from the alkene fragment is systematically stronger than the backdonation interaction ($\Delta E(\rho_1) > \Delta E(\rho_2)$) regardless of the substituent present in the alkene (see Table 2). As expected, the donation from the alkene becomes stronger when donor groups are attached to the C=C double bond (see for instance, complexes derived from isobutene, **7**, or **MCB**, **8**). In contrast, the backdonation ρ_2 becomes clearly weaker for those complexes having good

donor substituents (i.e. complexes **7** or **8**) whereas species having electron-withdrawing groups (i.e. complexes derived from CF₃-substituted alkenes **2** or **3**) and also the ACP group, exhibit much higher backdonations. This trend in the backdonation roughly matches the trend computed for the barriers associated with the anti-Markovnikov addition (see Table 2). For this reason, a very good linear relationship was found when plotting the computed barriers versus the energies associated with the [Au]⁺→ $\pi^*(C=C)$ backdonation (correlation coefficient of 0.98, Figure 6). This linear correlation therefore indicates that the higher the ability of the alkene for accepting electron density from the transition metal fragment, the higher the backdonation (more negative values) and the lower the anti-Markovnikov Gibbs energy barrier. It can be then concluded that the $\Delta E(\rho_2)$ values given by the EDA-NOCV method can be used as a reliable, quantitative measure of the barrier associated with the anti-Markovnikov addition, which ultimately determines the regioselectivity of the transformation.

Table 2. Computed NOCV stabilization energies $\Delta E(\rho)$ (in kcal/mol) present in the initial [AuP1⁺]-alkene complexes.[a]

alkene	$\Delta E(\rho_1)$	$\Delta E(\rho_2)$	$\Delta G_{\text{aM}}^\ddagger$
2	−25.4	−21.9	8.1
3	−28.6	−19.4	10.6
4	−29.7	−15.6	16.1
5	−32.6	−13.3	19.4
6 (b-ACP)	−30.9	−13.1	21.0
7	−33.1	−10.7	27.4

8 (MCB)	-33.2	-10.7	27.3
----------------	-------	-------	------

^[a] All data have been computed at the ZORA-BP86-D3/TZ2P//M06/6-31G(d,p)&SDD(f) level.

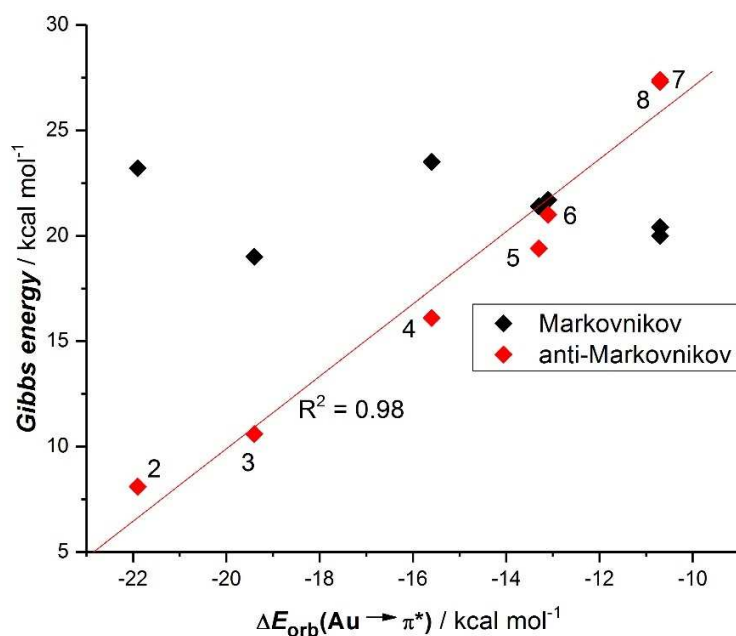


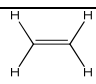
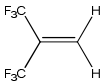
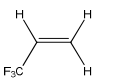
Figure 6. Plot of backdonation energies versus relative Gibbs energy of Markovnikov (black squares) and anti-Markovnikov (red squares) addition. Energy values refer to entries in Table 2.

Effect of modifying the L ligand on the [L-Au(I)]⁺ catalyst

The effect of modifying the ligand of the catalyst was computationally assessed next. The nucleophilic addition on the chosen eight alkenes was studied by using as catalyst a gold(I) complex with two additional ligands: the trimethylphosphine (PMe₃), which is a stronger electron-donor phosphine than P1-phosphine, and an abnormal N-heterocyclic carbene (*sa*), which is also a more electron-donating ligand (see Scheme 2).

The trimethylphosphine (PMe_3) was selected because it is one of the best electron-donating phosphine ligands. According to the tendency found in the previous section, i.e. higher backdonation results into a lower anti-Markovnikov barrier (Figure 6), it was expected that the use of this ligand should improve the regioselectivity for the anti-Markovnikov product compared to the P1 ligand. The Gibbs energy barriers for both Markovnikov and anti-Markovnikov additions obtained as well as the difference energies are collected in Table 3. Comparing the data in Table 3 (PMe_3 ligand) and Table 1 (P1 ligand), it can be observed that, the Gibbs energy barrier for both Markovnikov and anti-Markovnikov nucleophilic additions generally decreases when replacing the P1 ligand by the trimethylphosphine ligand (PMe_3). Nevertheless, even though the anti-Markovnikov barrier decreases with the PMe_3 ligand, in all cases the reduction of the Markovnikov barriers is systematically higher than that for the anti-Markovnikov addition. As a consequence, anti-Markovnikov hydroamination is not enhanced with this ligand but the opposite tendency is found.

Table 3. Gibbs energy barriers (Markovnikov, $\Delta G_{\text{M}}^\ddagger$ and anti-Markovnikov, $\Delta G_{\text{aM}}^\ddagger$, in kcal/mol) for the *anti* nucleophilic attack catalyzed by $[\text{Au}(\text{PMe}_3)]^+$ and geometrical parameters (in Å) for their initial intermediates (π -coordinated alkenes).^[a]

Entry	Substrate	$\Delta G_{\text{M}}^\ddagger$	$\Delta G_{\text{aM}}^\ddagger$	$\Delta\Delta G^\ddagger$	$\mathbf{d}_1\text{--}\mathbf{d}_2^{[\text{b}]}$
1		14.4	-	-	0.001
2		18.4	6.0	12.4	0.046
3		16.3	8.7	7.6	0.022

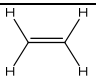
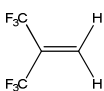
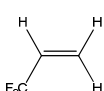
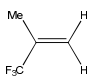
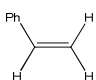
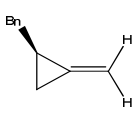
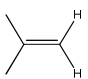
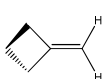
4		17.7	14.8	2.9	-0.080
5		17.1	18.5	-1.4	-0.152
6		19.9	21.8	-1.9	-0.130
7		19.2	27.4	-8.2	-0.230
8		16.9	24.8	-7.9	-0.252

^[a] All data have been computed at the M06/6-31G(d,p)&SDD(f) level.

^[b] d₁=distance Au-C_{terminal}; d₂= distance Au-C_{internal} from optimized structures.

Finally, the hydroamination reaction of alkenes was also analyzed by using the catalyst ligand *sa* (Scheme 2). We selected this particular ligand because it showed the best performance for the Au(I)-catalyzed hydrohydrazination of alkynes among different NHC ligands studied in a previous work,^{18c} in concordance with experiment.⁴⁴ The Gibbs energies for both Markovnikov and anti-Markovnikov nucleophilic additions for the hydroamination reaction of the same eight alkenes as well as the energy differences between both pathways are gathered in Table 4. Similar regioselectivity trends to those observed previously with the PMe₃ ligand are computed with this particular NHC ligand. Therefore, our calculations indicate that the anti-Markovnikov regioselectivity is lower using either the trimethylphosphine ligand (PMe₃) or the abnormal NHC ligand (*sa*) than the bulky P1 ligand.

Table 4. Gibbs energy barriers (Markovnikov, ΔG_M^\ddagger and anti-Markovnikov, ΔG_{aM}^\ddagger , in kcal/mol) for the *anti* nucleophilic attack catalyzed by $[\text{Au}(\text{sa})]^+$ and geometrical parameters (in Å) for their initial intermediates (π -coordinated alkenes).^[a]

Entry	Substrate	ΔG_M^\ddagger	ΔG_{aM}^\ddagger	$\Delta\Delta G^\ddagger$	$d_1-d_2^{[b]}$
1		16.9	-	-0.006	
2		21	5.6	15.4	0.037
3		18.4	11	7.4	0.020
4		21.1	15.4	5.7	-0.068
5		19.9	21.7	-1.8	-0.091
6		19.4	20.8	-1.4	-0.089
7		20.5	27.7	-7.2	-0.182
8		19.4	27	-7.6	-0.205

^[a] All data have been computed at the M06/6-31G(d,p)&SDD(f) level.

^[b] d_1 =distance Au-C_{terminal}; d_2 = distance Au-C_{internal} from optimized structures.

In order to check whether the regioselectivity can be also related to the coordination mode of the alkene for these two ligands (PMe_3 and sa), the difference of the distances between both carbon atoms of the alkene and the metal center (d_1-d_2) was plotted versus the energy difference between the Markovnikov and anti-Markovnikov additions ($\Delta\Delta G^\ddagger$). Once again, very good linear correlations were found for these hydroamination reactions catalyzed by the cationic $[\text{Au}(\text{PMe}_3)]^+$ and $[\text{Au}(\text{sa})]^+$ complexes (Figure 7), which further support that the coordination mode of the initial π -complex determines the regioselectivity outcome of the transformation

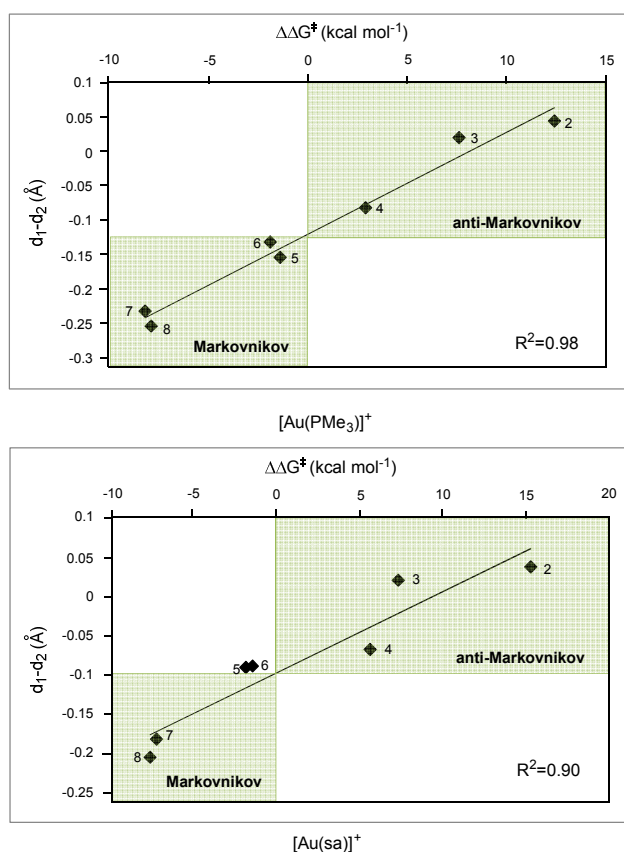


Figure 7. Plot of difference in Gibbs energy between Markovnikov and anti-Markovnikov addition barriers ($\Delta\Delta G^\ddagger$) versus the difference in the distance of both carbon atoms of alkene and the metal

center (d_1 – d_2 parameter) for hydroamination of alkenes catalyzed by $[\text{Au}(\text{PMe}_3)]^+$ (top) and $[\text{Au}(\text{sa})]^+$ (bottom).

CONCLUSIONS

The complete reaction mechanism for the hydroamination of 1-benzyl-2-methylenecyclopropane (**b-ACP**) with an urea-based amine catalyzed by the cationic $[\text{Au}(\text{I})\text{-P1}]^+$ complex was explored by means of DFT calculations. The involved mechanism can be described as a typical π -catalysis activation mechanism. Therefore, the first step of the process involves the coordination of the alkene to the metal center followed by the nucleophilic addition of the amine to the activated alkene. This step constitutes the rate determining step for both Markovnikov and anti-Markovnikov reaction pathways. Then, a final protodeauration reaction of the corresponding alkenyl gold(I) intermediate, which is assisted by a second amine molecule, occurs to generate the hydroaminated product. For this particular alkene, the anti-Markovnikov addition is kinetically preferred, which is fully consistent with the experimental observations. According to the ASM approach, this is due to the comparatively lower deformation energy required by the initial π -complex to adopt the anti-Markovnikov transition state structure, which offsets the stronger interaction energy between the deformed fragments for the alternative Markovnikov pathway.

In addition, it was found that subtle modifications of the electronic nature of the alkene are translated into dramatic changes in the regioselectivity of the process. Thus, the energy barrier for the anti-Markovnikov addition significantly decreases when the capacity of the alkene for accepting electronic density from the transition metal fragment increases. Indeed, a nice correlation between the backbonding ability of the alkene and the Gibbs energy barrier for the anti-

Markovnikov route is found. The replacement of the P1 ligand by good donor ligands such as trimethylphosphine (PMe₃) or the *sa* abnormal N-heterocyclic carbene leads to a reduction of the anti-Markovnikov regioselectivity with respect to the P1 ligand.

Strikingly, the difference between the Markovnikov and anti-Markovnikov barriers can be directly estimated by a geometrical parameter that measures the degree of slippage of the alkene in the π -coordinated intermediate. Indeed, the geometrical distortion induced by the coordination of the alkene to the gold(I)-catalyst not only affects the extent of the required strain energy to adopt the corresponding transition state structure but also, the strength of the main orbital interactions (i.e. donation and backdonation) between the alkene and the catalyst. Therefore, it can be concluded that the coordination mode of the initial π -complex ultimately dictates the regioselectivity of this important transformation.

AUTHOR INFORMATION

Corresponding Author

* e-mail: agusti@klignon.uab.es (A.L.); israel@quim.ucm.es (I.F.); gregori.ujaque@uab.cat (G.U.).

Author Contributions

The manuscript was written through contributions of all authors. All authors have given approval to the final version of the manuscript.

ASSOCIATED CONTENT

Supporting Information. Cartesian coordinates of the optimized structures, absolute energies, and Gibbs energies in 1,4-dioxane (Hartrees) of all the calculated species. This material is available free of charge via the Internet at <http://pubs.acs.org>.

ACKNOWLEDGMENT

The authors acknowledge the financial support of the Spanish MINECO-FEDER (Grants CTQ2017-87889-P, CTQ2016-78205-P, CTQ2016-81797-REDC and FPI fellowship to A.C.-R.).

REFERENCES

- (1) (a) Huang, L.; Arndt, M.; Gooßen, K.; Heydt, H.; Gooßen, L. J., Late transition metal-catalyzed hydroamination and hydroamidation. *Chem. Rev.* **2015**, *115*, 2596-2697; (b) Müller, T. E.; Hultsch, K. C.; Yus, M.; Foubelo, F.; Tada, M., Hydroamination: Direct addition of amines to alkenes and alkynes. *Chem. Rev.* **2008**, *108*, 3795-3892.
- (2) Bernoud, E.; Lepori, C.; Mellah, M.; Schulz, E.; Hannedouche, J., Recent advances in metal free- and late transition metal-catalysed hydroamination of unactivated alkenes. *Catal. Sci. Technol.* **2015**, *5*, 2017-2037.
- (3) (a) Roesky, P. W.; Müller, T. E., Enantioselective catalytic hydroamination of alkenes. *Angew. Chem. Int. Ed.* **2003**, *42*, 2708-2710; (b) Alonso, F.; Beletskaya, I. P.; Yus, M., Transition-metal-catalyzed addition of heteroatom-hydrogen bonds to alkynes. *Chem. Rev.* **2004**, *104*, 3079-3160; (c) Hultsch, K. C., Transition metal-catalyzed asymmetric hydroamination of alkenes (AHA). *Adv. Synth. Catal.* **2005**, *347*, 367-391; (d) Severin, R.; Doye, S., The catalytic hydroamination of alkynes. *Chem. Soc. Rev.* **2007**, *36*, 1407-1420.
- (4) Hesp, K. D.; Stradiotto, M., Rhodium- and Iridium-catalyzed hydroamination of alkenes. *ChemCatChem* **2010**, *2*, 1192-1207.
- (5) (a) Zhang, J.; Yang, C.-G.; He, C., Gold(I)-catalyzed intra- and intermolecular hydroamination of unactivated olefins. *J. Am. Chem. Soc.* **2006**, *128*, 1798-1799; (b) Giner, X.; Nájera, C., (Triphenyl phosphite)gold(I)-catalyzed intermolecular hydroamination of alkenes and 1,3-dienes. *Org. Lett.* **2008**, *10*, 2919-2922; (c) Zhang, X.; Corma, A., Efficient addition of alcohols, amines and phenol to unactivated alkenes by au(III) or pd(II) stabilized by CuCl₂. *Dalton Trans.* **2008**, 397-403; (d) Zhang, Z.; Lee, S. D.; Widenhoefer, R. A., Intermolecular hydroamination of ethylene and 1-alkenes with cyclic ureas catalyzed by achiral and chiral gold(I) complexes. *J. Am. Chem. Soc.* **2009**, *131*, 5372-5373; (e) Timmerman, J. C.; Laulhé, S.; Widenhoefer, R. A., Gold(I)-catalyzed intramolecular hydroamination of unactivated terminal and internal alkenes with 2-pyridones. *Org. Lett.* **2017**, *19*, 1466-1469; (f) Abadie, M.-A.; Trivelli, X.; Medina, F.; Duhal, N.; Kouach, M.; Linden, B.; Génin, E.; Vandewalle, M.; Capet,

- F.; Roussel, P.; Del Rosal, I.; Maron, L.; Agbossou-Niedercorn, F.; Michon, C., Gold(I)-catalysed asymmetric hydroamination of alkenes: A silver- and solvent-dependent enantiodivergent reaction. *Chem. Eur. J.* **2017**, *23*, 10777-10788.
- (6) Haggin, J., Chemists seek greater recognition for catalysis. *Chem. Eng. News* **1993**, *71*, 23-27.
- (7) (a) Beller, M.; Seayad, J.; Tillack, A.; Jiao, H., Catalytic markovnikov and anti-markovnikov functionalization of alkenes and alkynes: Recent developments and trends. *Angew. Chem. Int. Ed.* **2004**, *43*, 3368-3398;(b) Ryu, J.-S.; Li, G. Y.; Marks, T. J., Organolathanide-catalyzed regioselective intermolecular hydroamination of alkenes, alkynes, vinylarenes, di- and trivinylarenes, and methylenecyclopropanes. Scope and mechanistic comparison to intramolecular cyclohydroaminations. *J. Am. Chem. Soc.* **2003**, *125*, 12584-12605;(c) Germain, S.; Lecoq, M.; Schulz, E.; Hannedouche, J., Lithium-catalyzed anti-Markovnikov intermolecular hydroamination reactions of vinylarenes and simple secondary amines. *ChemCatChem* **2017**, *9*, 1749-1753;(d) Zhu, S.; Buchwald, S. L., Enantioselective cuh-catalyzed anti-markovnikov hydroamination of 1,1-disubstituted alkenes. *J. Am. Chem. Soc.* **2014**, *136*, 15913-15916;(e) Bronner, S. M.; Grubbs, R. H., Formal anti-Markovnikov hydroamination of terminal olefins. *Chem. Sci.* **2014**, *5*, 101-106;(f) Ensign, S. C.; Venable, E. P.; Kortman, G. D.; Weir, L. J.; Hull, K. L., Anti-Markovnikov hydroamination of homoallylic amines. *J. Am. Chem. Soc.* **2015**, *137*, 13748-13751;(g) Strom, A. E.; Balcells, D.; Hartwig, J. F., Synthetic and computational studies on the Rhodium-catalyzed hydroamination of aminoalkenes. *ACS Catal.* **2016**, *6*, 5651-5665;(h) Musacchio, A. J.; Lainhart, B. C.; Zhang, X.; Naguib, S. G.; Sherwood, T. C.; Knowles, R. R., Catalytic intermolecular hydroaminations of unactivated olefins with secondary alkyl amines. *Science* **2017**, *355*, 727-730.
- (8) (a) Nguyen, T. M.; Nicewicz, D. A., Anti-Markovnikov hydroamination of alkenes catalyzed by an organic photoredox system. *J. Am. Chem. Soc.* **2013**, *135*, 9588-9591;(b) Nguyen, T. M.; Manohar, N.; Nicewicz, D. A., Anti-markovnikov hydroamination of alkenes catalyzed by a two-component organic photoredox system: Direct access to phenethylamine derivatives. *Angew. Chem. Int. Ed.* **2014**, *53*, 6198-6201;(c) Zhu, Q.; Graff, D. E.; Knowles, R. R., Intermolecular anti-markovnikov hydroamination of unactivated alkenes with sulfonamides enabled by proton-coupled electron transfer. *J. Am. Chem. Soc.* **2018**, *140*, 741-747.
- (9) Timmerman, J. C.; Robertson, B. D.; Widenhoefer, R. A., Gold-catalyzed intermolecular anti-Markovnikov hydroamination of alkylidenecyclopropanes. *Angew. Chem. Int. Ed.* **2015**, *54*, 2251-2254.
- (10) Timmerman, J. C.; Widenhoefer, R. A., Gold-catalyzed intermolecular anti-Markovnikov hydroamination of methylenecyclopropanes with 2-pyridones. *Adv. Synth. Catal.* **2015**, *357*, 3703-3706.
- (11) (a) Thibodeaux, C. J.; Chang, W.-C.; Liu, H.-W., Enzymatic chemistry of cyclopropane, epoxide, and aziridine biosynthesis. *Chem. Rev.* **2012**, *112*, 1681-1709;(b) Pietruszka, J., Synthesis and properties of oligocyclopropyl-containing natural products and model compounds. *Chem. Rev.* **2003**, *103*, 1051-1070;(c) Yu, L.-Z.; Chen, K.; Zhu, Z.-Z.; Shi, M., Recent advances in the chemical transformations of functionalized alkylidenecyclopropanes (FACPs). *Chem. Commun.* **2017**, *53*, 5935-5945.
- (12) (a) Fernández, I.; Cossío, F. P., Applied computational chemistry. *Chem. Soc. Rev.* **2014**, *43*, 4906-4908;(b) Tantillo, D. J., Faster, catalyst! React! React! Exploiting computational chemistry for catalyst development and design. *Acc. Chem. Res.* **2016**, *49*, 1079-1079.

- (13) (a) Kumar, R.; Katari, M.; Choudhary, A.; Rajaraman, G.; Ghosh, P., Computational insight into the hydroamination of an activated olefin, as catalyzed by a 1,2,4-triazole-derived nickel(II) n-heterocyclic carbene complex. *Inorg. Chem.* **2017**, *56*, 14859-14869;(b) Merz, L. S.; Wadepohl, H.; Clot, E.; Gade, L. H., Dehydrogenative coupling of 4-substituted pyridines mediated by a zirconium(ii) synthon: Reaction pathways and dead ends. *Chem. Sci.* **2018**, *9*, 5223-5232;(c) Marcos, R.; Bertini, F.; Rinkevicius, Z.; Peruzzini, M.; Gonsalvi, L.; Ahlquist, M. S. G., Mechanistic studies on NaHCO₃ hydrogenation and HCOOH dehydrogenation reactions catalysed by a FeII linear tetraphosphine complex. *Chem. Eur. J.* **2018**, *24*, 5366-5372.
- (14) Wang, C.; Ren, X.-R.; Qi, C.-Z.; Yu, H.-Z., Mechanistic study on gold-catalyzed highly selective hydroamination of alkylidenecyclopropanes. *J. Org. Chem.* **2016**, *81*, 7326-7335.
- (15) Brooner, R. E. M.; Widenhoefer, R. A., Cationic, two-coordinate gold π complexes. *Angew. Chem. Int. Ed.* **2013**, *52*, 11714-11724.
- (16) Zuccaccia, D.; Belpassi, L.; Macchioni, A.; Tarantelli, F., Ligand effects on bonding and ion pairing in cationic gold(I) catalysts bearing unsaturated hydrocarbons. *Eur. J. Inorg. Chem.* **2013**, *2013*, 4121-4135.
- (17) (a) Hashmi, A. S. K., Homogeneous gold catalysis beyond assumptions and proposals—characterized intermediates. *Angew. Chem. Int. Ed.* **2010**, *49*, 5232-5241;(b) Obradors, C.; Echavarren, A. M., Intriguing mechanistic labyrinths in gold(I) catalysis. *Chem. Commun.* **2014**, *50*, 16-28;(c) Soriano, E.; Fernández, I., Allenes and computational chemistry: From bonding situations to reaction mechanisms. *Chem. Soc. Rev.* **2014**, *43*, 3041-3105.
- (18) (a) Kovács, G.; Ujaque, G.; Lledós, A., The reaction mechanism of the hydroamination of alkenes catalyzed by gold(I)–phosphine: The role of the counterion and the N-nucleophile substituents in the proton-transfer step. *J. Am. Chem. Soc.* **2008**, *130*, 853-864;(b) Kovács, G.; Lledós, A.; Ujaque, G., Mechanistic comparison of acid- and gold(I)-catalyzed nucleophilic addition reactions to olefins. *Organometallics* **2010**, *29*, 5919-5926;(c) Couce-Rios, A.; Kovács, G.; Ujaque, G.; Lledós, A., Hydroamination of C–C multiple bonds with hydrazine catalyzed by N-heterocyclic carbene–gold(I) complexes: Substrate and ligand effects. *ACS Catal.* **2015**, *5*, 815-829;(d) Lepori, C.; Gómez-Orellana, P.; Ouharzoune, A.; Guillot, R.; Lledós, A.; Ujaque, G.; Hannedouche, J., Well-defined β -diketiminatocobalt(II) complexes for alkene cyclohydroamination of primary amines. *ACS Catal.* **2018**, *8*, 4446-4451.
- (19) Gaussian 09, R. B.1, Frisch, M. J.; Trucks, G. W.; Schlegel, H. B.; Scuseria, G. E.; Robb, M. A.; Cheeseman, J. R.; Scalmani, G.; Barone, V.; Mennucci, B.; Petersson, G. A.; Nakatsuji, H.; Caricato, M.; Li, X.; Hratchian, H. P.; Izmaylov, A. F.; Bloino, J.; Zheng, G.; Sonnenberg, J. L.; Hada, M.; Ehara, M.; Toyota, K.; Fukuda, R.; Hasegawa, J.; Ishida, M.; Nakajima, T.; Honda, Y.; Kitao, O.; Nakai, H.; Vreven, T.; Montgomery, Jr., J. A.; Peralta, J. E.; Ogliaro, F.; Bearpark, M.; Heyd, J. J.; Brothers, E.; Kudin, K. N.; Staroverov, V. N.; Kobayashi, R.; Normand, J.; Raghavachari, K.; Rendell, A.; Burant, J. C.; Iyengar, S. S.; Tomasi, J.; Cossi, M.; Rega, N.; Millam, N. J.; Klene, M.; Knox, J. E.; Cross, J. B.; Bakken, V.; Adamo, C.; Jaramillo, J.; Gomperts, R.; Stratmann, R. E.; Yazyev, O.; Austin, A. J.; Cammi, R.; Pomelli, C.; Ochterski, J. W.; Martin, R. L.; Morokuma, K.; Zakrzewski, V. G.; Voth, G. A.; Salvador, P.; Dannenberg, J. J.; Dapprich, S.; Daniels, A. D.; Farkas, Ö.; Foresman, J. B.; Ortiz, J. V.; Cioslowski, J.; Fox, D. J. Gaussian, Inc., Wallingford CT, 2009.
- (20) Zhao, Y.; Truhlar, D. G., The M06 suite of density functionals for main group thermochemistry, thermochemical kinetics, noncovalent interactions, excited states, and transition elements: Two new functionals and systematic testing of four M06-class functionals and 12 other functionals. *Theor. Chem. Acc.* **2008**, *120*, 215-241.

- (21) (a) Andrae, D.; Häußermann, U.; Dolg, M.; Stoll, H.; Preuß, H., Energy-adjusted ab initio pseudopotentials for the second and third row transition elements. *Theor. Chim. Acta* **1990**, *77*, 123-141;(b) Ehlers, A. W.; Böhme, M.; Dapprich, S.; Gobbi, A.; Höllwarth, A.; Jonas, V.; Köhler, K. F.; Stegmann, R.; Veldkamp, A.; Frenking, G., A set of f-polarization functions for pseudo-potential basis sets of the transition metals Sc-Cu, Y-Ag and La-Au. *Chem. Phys. Lett.* **1993**, *208*, 111-114.
- (22) Marenich, A. V.; Cramer, C. J.; Truhlar, D. G., Universal solvation model based on solute electron density and on a continuum model of the solvent defined by the bulk dielectric constant and atomic surface tensions. *J. Phys. Chem. B* **2009**, *113*, 6378-6396.
- (23) Gonzalez, C.; Schlegel, H. B., Reaction path following in mass-weighted internal coordinates. *J. Phys. Chem.* **1990**, *94*, 5523-5527.
- (24) ADF2017, scm, theoretical chemistry, vrije universiteit, amsterdam, the netherlands, <http://www.Scm.Coml>.
- (25) (a) Vosko, S. H.; Wilk, L.; Nusair, M., Accurate spin-dependent electron liquid correlation energies for local spin density calculations: A critical analysis. *Can. J. Phys.* **1980**, *58*, 1200-1211;(b) Becke, A. D., Density-functional exchange-energy approximation with correct asymptotic behavior. *Phys. Rev. A* **1988**, *38*, 3098-3100;(c) Perdew, J. P., Erratum: Density-functional approximation for the correlation energy of the inhomogeneous electron gas. *Phys. Rev. B* **1986**, *34*, 7406-7406.
- (26) (a) Grimme, S., Semiempirical GGA-type density functional constructed with a long-range dispersion correction. *J. Comput. Chem.* **2006**, *27*, 1787-1799;(b) Grimme, S.; Antony, J.; Ehrlich, S.; Krieg, H., A consistent and accurate ab initio parametrization of density functional dispersion correction (DFT-D) for the 94 elements H-Pu. *J. Chem. Phys.* **2010**, *132*, 154104.
- (27) (a) Van Lenthe, E.; Baerends, E. J., Optimized slater-type basis sets for the elements 1–118. *J. Comput. Chem.* **2003**, *24*, 1142-1156;(b) Franchini, M.; Philipsen, P. H. T.; van Lenthe, E.; Visscher, L., Accurate coulomb potentials for periodic and molecular systems through density fitting. *J. Chem. Theory Comput.* **2014**, *10*, 1994-2004.
- (28) (a) Lenthe, E. v.; Baerends, E. J.; Snijders, J. G., Relativistic regular two-component hamiltonians. *J. Chem. Phys.* **1993**, *99*, 4597-4610;(b) Lenthe, E. v.; Baerends, E. J.; Snijders, J. G., Relativistic total energy using regular approximations. *J. Chem. Phys.* **1994**, *101*, 9783-9792.
- (29) (a) Kovács, G.; Lledós, A.; Ujaque, G., Reaction mechanism of the gold(I)-catalyzed addition of phenols to olefins: A concerted process accelerated by phenol and water. *Organometallics* **2010**, *29*, 3252-3260;(b) BabaAhmadi, R.; Ghanbari, P.; Rajabi, N. A.; Hashmi, A. S. K.; Yates, B. F.; Ariafard, A., A theoretical study on the protodeauration step of the gold(I)-catalyzed organic reactions. *Organometallics* **2015**, *34*, 3186-3195;(c) Jin, L.; Wu, Y.; Zhao, X., Theoretical insight into the Au(I)-catalyzed hydration of halo-substituted propargyl acetate: Dynamic water-assisted mechanism. *RSC Advances* **2016**, *6*, 89836-89846.
- (30) (a) Balcells, D.; Ujaque, G.; Fernandez, I.; Khier, N.; Maseras, F., Mechanism of the base-assisted displacement of chloride by alcohol in sulfinyl derivatives. *J. Org. Chem.* **2006**, *71*, 6388-6396;(b) Balcells, D.; Ujaque, G.; Fernández, I.; Khier, N.; Maseras, F., How does the achiral base decide the stereochemical outcome in the dynamic kinetic resolution of sulfinyl chlorides? A computational study. *Adv. Synth. Catal.* **2007**, *349*, 2103-2110;(c) Simón, L.; Muñiz, F. M.; Sáez, S.; Raposo, C.; Morán, J. R., Enzyme mimics for michael additions with novel proton transport groups. *Eur. J. Org. Chem.* **2008**, *2008*, 2397-2403;(d) Simón, L.; Goodman, J. M., What is the mechanism of amine conjugate additions to pyrazole crotonate catalyzed by thiourea catalysts? *Org. Biomol. Chem.* **2009**, *7*, 483-487.

- (31) (a) Appelhans, L. N.; Zuccaccia, D.; Kovacevic, A.; Chianese, A. R.; Miecznikowski, J. R.; Macchioni, A.; Clot, E.; Eisenstein, O.; Crabtree, R. H., An anion-dependent switch in selectivity results from a change of C–H activation mechanism in the reaction of an imidazolium salt with $\text{IrH}_5(\text{PPh}_3)_2$. *J. Am. Chem. Soc.* **2005**, *127*, 16299-16311;(b) Davies, D. L.; Donald, S. M. A.; Macgregor, S. A., Computational study of the mechanism of cyclometalation by palladium acetate. *J. Am. Chem. Soc.* **2005**, *127*, 13754-13755;(c) García-Cuadrado, D.; Braga, A. A. C.; Maseras, F.; Echavarren, A. M., Proton abstraction mechanism for the palladium-catalyzed intramolecular arylation. *J. Am. Chem. Soc.* **2006**, *128*, 1066-1067;(d) D'Amore, L.; Ciancaleoni, G.; Belpassi, L.; Tarantelli, F.; Zuccaccia, D.; Belanzoni, P., Unraveling the anion/ligand interplay in the reaction mechanism of gold(I)-catalyzed alkoxylation of alkynes. *Organometallics* **2017**, *36*, 2364-2376.
- (32) $\Delta G_{\text{binding}}$ of **b-ACP** to $[\text{Au}(\text{P}1)]^+$ -catalyst is $-23.9 \text{ kcal}\cdot\text{mol}^{-1}$.
- (33) Calculations at DLNPO-CCSD(T)/cc-pVTZ&SDD level including solvent effects show a preference of 2.8 kcal/mol for the anti-markovnikov addition, in agreement with the observed experimental ratio of >25:1. For the method see: Riplinger, C.; Sandhoefer, B.; Hansen, A.; Neese, F. Natural triple excitations in local coupled cluster calculations with pair natural orbitals. *J. Chem. Phys.* **2013**, *139*, 134101.
- (34) Styrene hydroamination have been experimentally performed with a slightly different gold(I) complex $[(\text{L})\text{AuCl}]$ catalyst; L =2-di-tert-butylphosphino-1,1'-binaphthyl] obtaining the markovnikov product; see ref 5d.
- (35) Eisenstein, O.; Hoffmann, R., Activation of a coordinated olefin toward nucleophilic attack. *J. Am. Chem. Soc.* **1980**, *102*, 6148-6149.
- (36) Eisenstein, O.; Hoffmann, R., Transition-metal complexed olefins: How their reactivity toward a nucleophile relates to their electronic structure. *J. Am. Chem. Soc.* **1981**, *103*, 4308-4320.
- (37) Barone, C. R.; Cini, R.; Clot, E.; Eisenstein, O.; Maresca, L.; Natile, G.; Tamasi, G., A NMR, X-ray, and DFT combined study on the regio-chemistry of nucleophilic addition to platinum(II) coordinated terminal olefins. *J. Organomet. Chem.* **2008**, *693*, 2819-2827.
- (38) Couce-Rios, A.; Lledós, A.; Ujaque, G., The origin of anti-markovnikov regioselectivity in alkene hydroamination reactions catalyzed by $[\text{Rh}(\text{DPEphos})]^+$. *Chem. Eur. J.* **2016**, *22*, 9311-9320.
- (39) (a) van Zeist, W.-J.; Bickelhaupt, F. M., The activation strain model of chemical reactivity. *Org. Biomol. Chem.* **2010**, *8*, 3118-3127;(b) Fernández, I.; Bickelhaupt, F. M., The activation strain model and molecular orbital theory: Understanding and designing chemical reactions. *Chem. Soc. Rev.* **2014**, *43*, 4953-4967;(c) Wolters, L. P.; Bickelhaupt, F. M., The activation strain model and molecular orbital theory. *WIREs Comput. Mol. Sci.* **2015**, *5*, 324-343;(d) Bickelhaupt, F. M.; Houk, K. N., Analyzing reaction rates with the distortion/interaction-activation strain model. *Angew. Chem. Int. Ed.* **2017**, *56*, 10070-10086;(e) See also: I. Fernández, in *discovering the future of molecular sciences* (Ed.: B. Pignataro), Wiley-VCH, Weinheim, 2014, pp. 165–187.
- (40) (a) Bickelhaupt, F. M.; Solà, M.; Fernández, I., Understanding the reactivity of endohedral metallofullerenes: C_{78} versus $\text{sc}_{3n}@\text{c}_{78}$. *Chem. Eur. J.* **2015**, *21*, 5760-5768;(b) García-Rodeja, Y.; Solà, M.; Bickelhaupt, F. M.; Fernández, I., Reactivity and selectivity of bowl-shaped polycyclic aromatic hydrocarbons: Relationship to c_{60} . *Chem. Eur. J.* **2016**, *22*, 1368-1378;(c) García-Rodeja, Y.; Solà, M.; Fernández, I., Understanding the reactivity of planar polycyclic aromatic hydrocarbons: Towards the graphene limit. *Chem. Eur. J.* **2016**, *22*, 10572-10580;(d)

Yepes, D.; Pérez, P.; Jaque, P.; Fernández, I., Effect of lewis acid bulkiness on the stereoselectivity of Diels–Alder reactions between acyclic dienes and α,β -enals. *Org. Chem. Front.* **2017**, *4*, 1390-1399; (e) Levandowski, B. J.; Hamlin, T. A.; Bickelhaupt, F. M.; Houk, K. N., Role of orbital interactions and activation strain (distortion energies) on reactivities in the normal and inverse electron-demand cycloadditions of strained and unstrained cycloalkenes. *J. Org. Chem.* **2017**, *82*, 8668-8675.

(41) Mitoraj, M. P.; Michalak, A.; Ziegler, T., A combined charge and energy decomposition scheme for bond analysis. *J. Chem. Theory Comput.* **2009**, *5*, 962-975.

(42) (a) Morokuma, K., Molecular orbital studies of hydrogen bonds. III. C=O \cdots H–O hydrogen bond in H₂CO \cdots H₂O and H₂CO \cdots 2H₂O. *J. Chem. Phys.* **1971**, *55*, 1236-1244; (b) Ziegler, T.; Rauk, A., On the calculation of bonding energies by the Hartree Fock Slater method. *Theor. Chim. Acta* **1977**, *46*, 1-10.

(43) García-Rodeja, Y.; Fernández, I., Understanding the effect of α -cationic phosphines and group 15 analogues on π -acid catalysis. *Organometallics* **2017**, *36*, 460-466.

(44) (a) Kinjo, R.; Donnadieu, B.; Bertrand, G., Gold-catalyzed hydroamination of alkynes and allenes with parent hydrazine. *Angew. Chem. Int. Ed.* **2011**, *50*, 5560-5563; (b) Martin, D.; Lassauque, N.; Donnadieu, B.; Bertrand, G., A cyclic diaminocarbene with a pyramidalized nitrogen atom: A stable N-heterocyclic carbene with enhanced electrophilicity. *Angew. Chem. Int. Ed.* **2012**, *51*, 6172-6175; (c) Hashmi, A. S. K.; Riedel, D.; Rudolph, M.; Rominger, F.; Oeser, T., Regioselective formation of saturated abnormal NHC–gold(I) complexes by [3+2] cycloaddition of azomethine ylides and isonitrile gold(I) complexes. *Chem. Eur. J.* **2012**, *18*, 3827-3830.

TABLE OF CONTENTS GRAPHIC

